Springer

KSME

Journal of Mechanical Science and Technology 24 (4) (2010) 865~871
www.springerlink.com/content/1738-494x
DOI 10.1007/s12206-010-0311-x

Characteristics of vertically injected buoyant jets of highly diluted propane †

K. W. Chun, J. Kim, S. H. Won and S. H. Chung*

School of Mechanical and Aerospace Engineering, Seoul National University, Seoul 151-742, Korea

(Manuscript Received October 8, 2008; Revised November 17, 2008; Accepted February 22, 2010)

Abstract

In coflow jets with the nozzle diameter of *O* (1 cm) and the fuel jet velocity of *O* (10 cm/s), the buoyancy induced by the density difference between the fuel and air influences the jet structure appreciably. The present study investigated the behavior of such a buoyant jet numerically and experimentally, especially when the fuel stream had higher density than air. When the fuel jet was composed of propane highly diluted with nitrogen, the fuel jet was decelerated and formed a stagnation region. Consequently, the fuel was carried downstream by the coflow having a circular cone shape. When the fuel was moderately diluted or as the jet velocity increased, numerical results showed the Kelvin-Helmholtz type instability along the mixing layer of the jet. When the fuel jet velocity was relatively high, the stagnation height increased nonlinearly with fuel jet velocity having the power of approximately 1.62. In the relatively high Reynolds number regime of Re > 80, the stagnation height can be correlated to $\mathrm{Re}^{0.62}\,\mathrm{Ri}^{-0.5}$, indicating the combined effects of buoyancy and jet momentum. As the Reynolds number becomes small, the stagnation height was affected by the streamwise diffusion due to fuel concentration gradient and by the wake behavior near the nozzle tip. Accordingly, the stagnation heights approach to none-zero values, which were found to be relatively insensitive to fuel dilution.

Keywords: Jets; Stability; Laminar flows; Buoyancy-driven

1. Introduction

Coflow jets of fuel and air with the fuel nozzle diameters of *O* (1 cm) and the fuel jet velocities of *O* (10 cm/s) have been frequently adopted in combustion studies to extract fundamental mechanisms underlying the phenomena, for example, to investigate diffusion flame structure, flame stabilization, and soot formation [1, 2]. These flames in a coflow are generally more stable over a free jet, which facilitates various laser diagnostics techniques.

In a recent experimental study on laminar lifted flames in a coflow jet, periodically oscillating lifted flames were observed when the propane fuel was highly diluted with nitrogen [3]. The frequency range was 2.5-4.0 Hz in a certain limited range of jet velocity. It has been demonstrated that the corresponding cold jets have a unique feature in the normal gravity condition, in that the upwardly injected fuel jet was decelerated and formed a stagnation region by the negative buoyancy acting on propane, which is heavier than the ambient air. Near the stagnation region, the fuel was convected radially and then carried downstream by the momentum of the coflow, by having a circular cone shape of fuel region. In contrast to the cold jet flow, the reacting flow with a lifted flame did not show a stagnation region due to the positive buoyancy force exerted on the burnt gases.

Based on these observations of the unique characteristics of negatively buoyant jets, the present study investigated the behavior of buoyant cold jets both numerically and experimentally, especially when the fuel has higher density than air.

2. Numerical calculation and experiment

To investigate the detailed flow field of buoyant jets in coflow, the numerical solver was based on the direct numerical simulation (DNS) code for axisymmetric flow [4, 5]. The time-dependent governing equations for the momentum and species in the cylindrical-coordinate (*r*, *z*) were solved with the low Mach number approximation [6], in such a way that the zeroth order pressure term was constant over the computational domain and the first order term was governed by the Poisson equation. To account for the buoyancy effect, the momentum equation included the gravitational acceleration term. A finite difference procedure on a staggered grid was adopted using a second-order central difference scheme. The second-order predictor-corrector algorithm was used for the time integration [7].

† This paper was recommended for publication in revised form by Associate Editor Ohchae Kwon

*Corresponding author. Tel.: +82 2 880 7114, Fax.: +82 2 883 0179
E-mail address: shchung@snu.ac.kr

A non-uniform grid system was adopted by embedding finer grids in the vicinity of a stagnation region. The nozzle rim protruded 10 mm from the inlet boundary to match the experiment. Consequently, the Poisson equation could not be directly solved with the spectral method, instead the multi-grid method was used in the axial direction as a fast iterative method. In the radial direction, the Poisson solver adopted the tri-diagonal matrix solver (TDMA). In the radial and vertical directions, the computation dimensions were 15 and 45-125 times the nozzle radius and the corresponding number of meshes were 65-129 and 256-833, respectively.

The time step was 0.1 ms to satisfy the general stability criteria that the invicid and viscous Courant-Friedrichs-Lewy numbers should be less than 1.0 and 0.5, respectively, for the second order explicit time integration and the central spatial difference scheme [6]. As inlet conditions, the fully developed velocity profile of pipe flow for the fuel stream was assumed and the uniform velocity profile for the coflow except near the inner tube wall where a thin boundary layer was assumed to satisfy the no-slip condition. At the outlet, all scalar variables and velocity vectors were evaluated from the convective boundary conditions. At the sidewall, zero fluxes of scalar variables and normal velocity were applied. Thermodynamic and transport properties were evaluated from the CHEMKIN-III and TRANSPORT Package [8, 9].

The experimental apparatus consisted of a coflow burner, a flow control system, and a visualization setup. The coflow burner had a central fuel nozzle with 11.1 mm i.d. and 350 mm in length for the flow inside to be fully developed. Coflow air was supplied to a coaxial nozzle with 154 mm i.d. through glass beads and a ceramic honeycomb to obtain uniform flow. The fuel was commercially-pure grade propane (> 99%) diluted with nitrogen. The flow rates of fuel and air were metered with mass flow controllers calibrated with a wet-test gas meter. To minimize outside disturbance, an optically accessible acrylic cylinder with 100 cm length surrounded the coflow air.

The flow field was visualized with a acetone planar laser induced fluorescence (PLIF) technique. The PLIF system consisted of an Nd:YAG laser (Continuum, PL8000) and a dye laser (Continuum, ND 6000). To capture the acetone PLIF images, an ICCD camera (Princeton Instrument, ICCD-MAX) was used. The acetone was excited at 280 nm and the fluorescence was detected in the visual range of 350 to 550 nm through optical filters. To further substantiate the effect of buoyancy, the flow field was also visualized with a planar Mie scattering from fine dust particles in the honeycomb.

3. Results and discussion

3.1 Jet behavior

At a certain degree of nitrogen dilution, the propane jet with coflow air shows a unique behavior compared to typical jets. The Mie scattering technique visualized this behavior for the propane mole fraction of $X_{F,o}$ = 0.1, the coflow velocity of V_{co} = 9.4 cm/s, and the fuel jet velocities of $U_{F,o}$ = 7.07 and 10.61 cm/s, as shown in Fig. 1. The propane jet decelerates by the buoyancy exerted on heavy fuel, such that a stagnation region is formed along the centerline. Then, the fuel flows radially outward and is carried downstream by the coflow air, having a circular cone shape of fuel region. This unique feature is due to the buoyancy effect, when the molecular weight of the fuel mixture is heavier than that of the coflow air. Note that for the laser beam access, there are two slits on the sides of the outer cylinder. Consequently, the conical shape is somewhat outwardly distorted by the air leakage through the slits, as compared to the case without having slits. In spite of this disturbance, the influence on the stagnation heights was minimal.

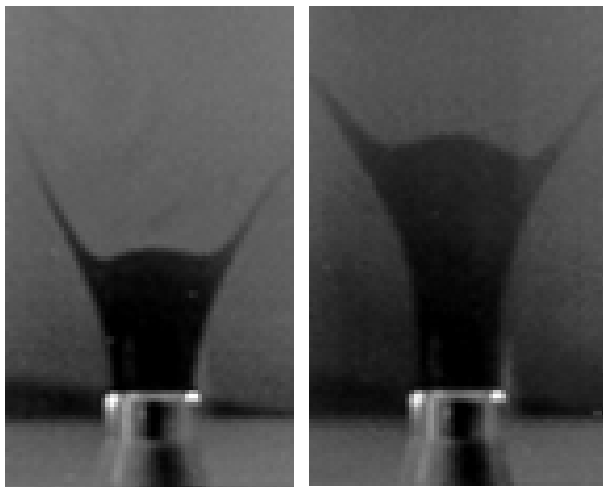

(a) (b)

Fig. 1. Mie scattering images demonstrating stagnation region for (a) $U_{F,o}$ = 7.07 cm/s and (b) 10.62 cm/s ($X_{F,o}$ = 0.1 and V_{co} = 9.4 cm/s).

The molecular weight of propane/nitrogen mixture increases linearly with the propane mole fraction. For $X_{F,o}$ = 0.0597, the molecular weight of the mixture becomes the same as that of air, that is, M_{mix} = 28.970 g/mol. Sample calculations have been performed for the cases with the mixture molecular weight either smaller or lager than that of air. Fig. 2 shows the numerical results of the distribution of propane mole fraction for $X_{F,o}$ = 0.05 and 0.10. For $X_{F,o}$ = 0.05, the molecular weight of 28.814 g/mol is lighter than that of air. In such a case, the flow maintains the typical structure of jets, that is, continuously decreasing fuel mass fraction and axial velocity in both axial and radial directions. For $X_{F,o}$ = 0.10, the molecular weight is 29.610 g/mol, which is heavier than air. Since the buoyancy force acting downward interacts with the upward jet momentum, the jet structure becomes highly distorted. The fuel concentration along the centerline decreases rapidly and a cone shaped fuel region exists in the downstream.

The acetone PLIF experiment has been conducted to visualize the concentration field by adding 0.1% of acetone seeded to the fuel stream. The measured acetone PLIF image and the numerically predicted concentration field for $X_{F,o}$ = 0.10 and

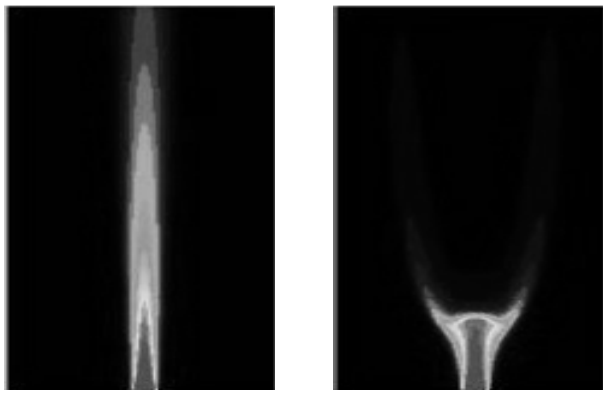

(a) (b)

Fig. 2. Concentration profiles of propane for (a) $X_{F,o}$ = 0.05 and (b) 0.10 ($U_{F,o}$ = 10.6 cm/s and V_{co} = 9.4 cm/s).

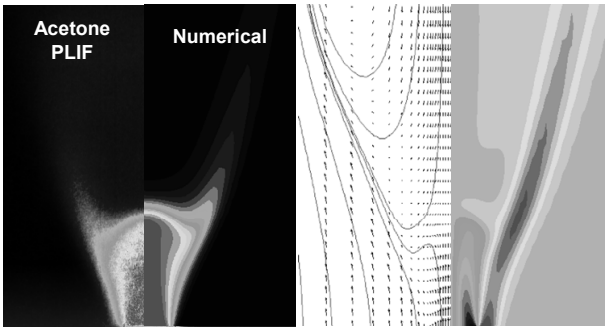

(a) (b) (c)

Fig. 3. Acetone PLIF image and numerical result for fuel concentration (a), streamlines (b) and vorticity field (c) ($X_{F,o}$ = 0.10, $U_{F,o}$ = 7.07 cm/s and V_{co} = 9.4 cm/s).

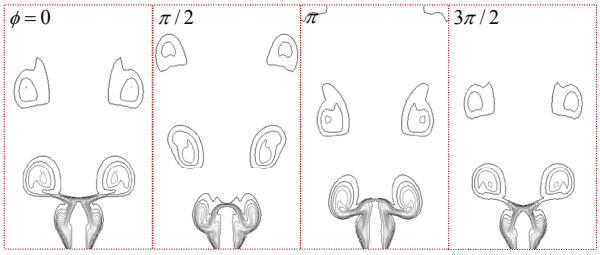

(a)

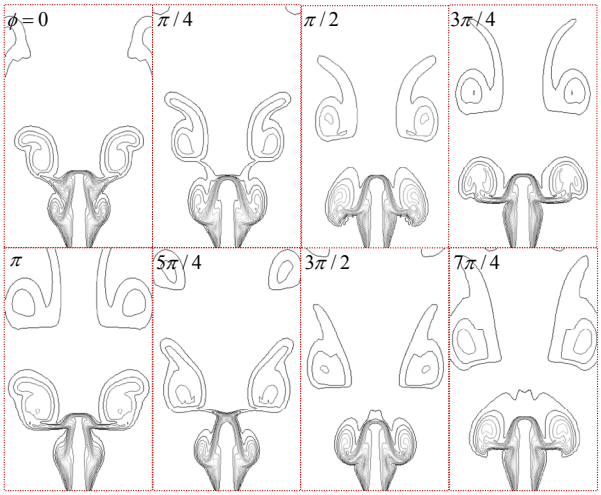

(b)

Fig. 4. Sequence of concentration profiles of propane for oscillating flow for (a) $U_{F,o}$ = 12.0 cm/s and (b) 16.0 cm/s ($X_{F,o}$ = 0.20 and V_{co} = 9.4 cm/s).

$U_{F,o}$ = 7.07 cm/s are compared in Fig. 3(a). Considering the effect of acetone addition on molecular weight and thermodynamic properties, the two results agree satisfactorily. The numerical predictions of the distributions of streamlines (b) and vortices (c) are also demonstrated. The axial velocity of the propane jet slows down due to the buoyancy effect and a stagnation region is formed along the centerline. Since the jet momentum cannot overcome the buoyancy, the propane flows radially near the stagnation point. Then, the momentum of coflow air carries the fuel stream along the shear layer. The vorticity field demonstrates strong vorticity regions near the jet exit by the Poiseuille flow in the tube and the boundary layer near the inner tube wall for the coflow. Also, strong vorticity is generated in the shear layer between the boundary of the recirculation zone and the coflow.

When the propane concentration and/or jet velocity becomes large, instability occurs in such a way that periodic solutions are obtained. Fig. 4(a) shows the sequence of oscillation in the concentration profiles of propane for $X_{F,o}$ = 0.20 and $U_{F,o}$ = 12.0 cm/s (case 1). The flow field oscillates with the frequency of 1.90 Hz. The instability grows along the mixing layer of the jet stem and a discrete vortex is shedded in the downstream. This phenomenon can be attributed to the Kelvin-Helmholtz type instability along the shear layer between the fuel jet and coflow. Fig. 4(b) shows the concentration profiles of propane for $X_{F,o}$ = 0.20 and $U_{F,o}$ = 16.0 cm/s (case 2), demonstrating the sequence of doubly-periodic oscillation. The vortex shedding occurs twice during one period of oscillation with the frequency of 1.55 Hz.

Fig. 5 shows the temporal variations of axial velocities at two monitoring points. The monitoring point A is selected near the stagnation region along the axis and point B is a location where the vortex is passing by. The results show that the flow field for the case 1 demonstrates a periodic oscillation, while the case 2 responds with a frequency-doubling.

Fig. 6 shows the concentration, streamlines and vorticity field at one instant for the case 1. The velocity field and streamlines show that vortices are generated in the shear layer region and are detached from the main jet in the downstream. The vorticity profile shows that negative (dotted lines) and positive (solid lines) vorticity regions are close by near the lower edge of vortices. Note that the positive vorticity region due to the difference in the velocities between the fuel jet and coflow is penetrated by the negative vorticity region due to the descending fuel near the stagnation region.

The experimental results of the acetone PLIF images for the

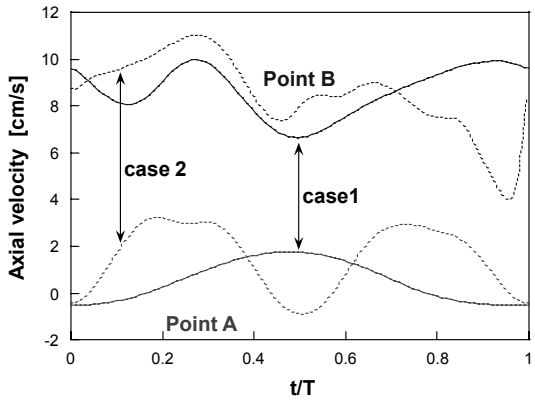

Fig. 5. Axial velocity variation during one cycle of oscillation at monitoring points for $X_{F,o}$ = 0.20 and V_{co} = 9.4 cm/s (case 1 for $U_{F,o}$ = 12.0 cm/s and case 2 for 16.0 cm/s).

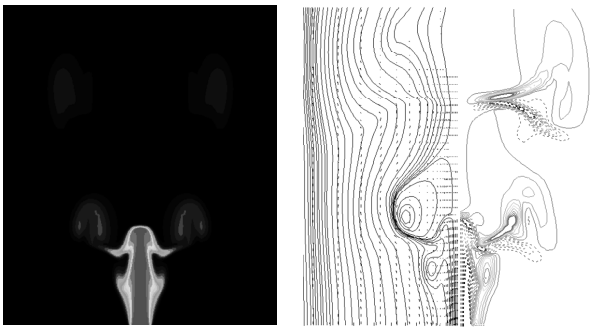

(a) (b) (c)

Fig. 6. Profiles of concentration (a), streamline (b) and vorticity (c) for oscillating flow at an instant ($X_{F,o}$ = 0.20, $U_{F,o}$ = 16.0 cm/s and V_{co} = 9.4 cm/s).

same condition as Fig. 4(b) is shown in Fig. 7. Both the confined (with the outer cylinder) and unconfined (without the outer cylinder) cases demonstrate the formation of discrete vortex along the shear layer. However, the structures show generally asymmetrical having three-dimensional nature. Due to the limitation of the axisymmetric numerical code, these three-dimensional structures cannot be predicted, even though the occurrence of instability along the shear layer can be reasonably predicted. The difference between the acetone PLIF images and the numerical results can also be partially attributed to the acetone seeding.

Numerically determined boundary between the steady and oscillating regions is shown in Fig. 8. When the propane concentration and/or jet velocity becomes large, the flow field oscillates in the numerical calculation. The jet velocity at the onset of oscillation decreases as the molecular weight or propane mole fraction increases.

3.2 Stagnation height

One of the interesting features of the present buoyant jet is the stagnation height H_s, that can be defined at the height where the axial velocity vanishes. Fig. 9 shows the variation

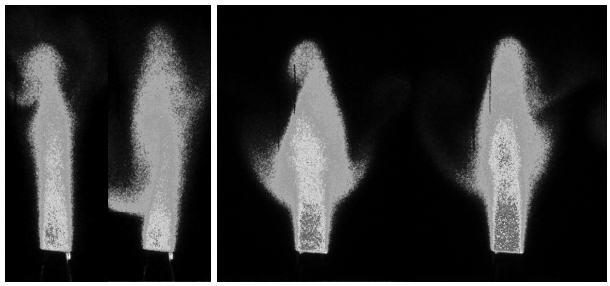

(a) (b)

Fig. 7. Acetone PLIF images for confined (a) and unconfined (b) cases ($X_{F,o}$ = 0.20, $U_{F,o}$ = 16.0 cm/s and V_{co} = 9.4 cm/s).

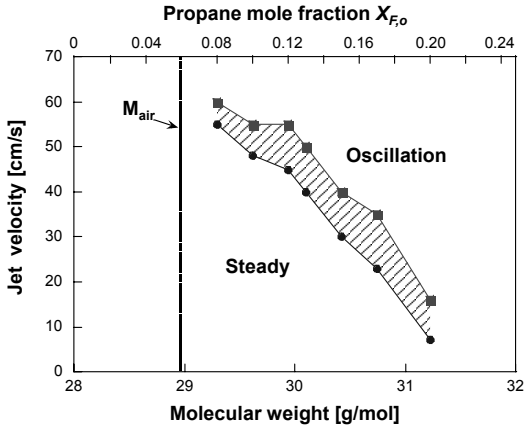

Fig. 8. Domain of oscillating region in terms of jet velocity and propane mole fraction (V_{co} = 9.4 cm/s).

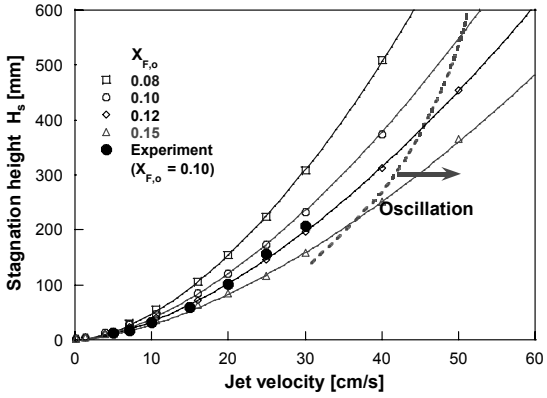

Fig. 9. Variation of stagnation height with jet velocity at various propane mole fractions.

of predicted stagnation heights with jet velocity at various propane mole fractions for V_{co} = 9.4 cm/s, where the stagnation height is defines numerically at the zero axial velocity. The stagnation height increases nonlinearly with jet velocity and increases with decreasing propane mole fraction. The domain of oscillation is also marked. Even though the vortex shedding changes temporal flow field significantly, the variation of stagnation height for specified $X_{F,o}$ and U_o is within 5%.

Experimentally determined stagnation height is also repre-

sented in Fig. 9, where the height is determined from the inflexion point of the concentration profile along the centerline in the acetone PLIF images. Considering the influences of acetone seeding and the two different definitions, the result agrees reasonably well with the numerical result. Note that the zero axial velocity condition of the stagnation height definition numerically is within 5% larger than the inflection point definition for the concentration.

One can also plot the stagnation height as a function of the Reynolds number $\mathrm{Re} = U_{F,o} d / v$, where v is the kinematic viscosity of mixture fuel. Since the variation of the kinematic viscosity is not significant for the range of $0.08 \le X_{F,o} \le 0.15$, the plot is qualitatively similar as Fig. 9. The stagnation height is curvefitted in the form of $(H_s/d) \propto \mathrm{Re}^n$ and the exponent is found to be in the range of $1.57 \le n \le 1.66$ for $0.08 \le X_{F,o} \le 0.15$ for moderately large Reynolds numbers of Re > 80. The characteristics for small Re will be discussed later.

The stagnation height will be influenced by the vertical fuel jet momentum and the fuel jet deceleration by the buoyancy due to the density difference between the fuel and air. The specific vertical jet momentum can be expressed as $\rho_{F,o} U_{F,o}$, where ρ is the density. The specific decelerating momentum can be expressed as the specific buoyancy force $\Delta\rho g$ multiplied by the characteristic deceleration time from the nozzle to the stagnation point, ($H_s / U_{F,o}$), where g is the gravitational acceleration and $\Delta\rho = \rho_{F,o} - \rho_{air}$. Since, H_s increases with $U_{F,o}$, while decreases with $\Delta\rho g$, the nondimensional stagnation height (H_s/d) is scaled with the ratio of the momenta as

$$\frac{H_s}{d} \times \frac{\Delta\rho g (H_s / U_{F,o})}{\rho_{F,o} U_{F,o}} = \left(\frac{H_s}{d}\right)^2 \times \left[\frac{\Delta\rho}{\rho_{F,o}} \frac{gd}{U_{F,o}^2}\right] = \left(\frac{H_s}{d}\right)^2 \times \mathrm{Ri} \qquad (1)$$

where the Richardson number, Ri, is defined as the ratio of buoyancy force to inertia force as $(\Delta\rho / \rho_{F,o})(gd / U_{F,o}^2)$. The non-dimensional stagnation height scaled with the square-root of the Richardson number $(H_s / d) \times \mathrm{Ri}^{1/2}$ is plotted in terms of Re in Fig. 10 for moderately large Reynolds numbers of Re > 80. The results exhibited a satisfactory correlation at various $X_{F,o}$ as

$$(H_s / d) \times \mathrm{Ri}^{1/2} = 0.120 \times \mathrm{Re}^{0.621} \qquad (2)$$

with the correlation coefficient of R = 0.993.

When the Reynolds number becomes small, the balance between the vertical jet momentum and the gravitational decelerating momentum cannot be maintained, since the axial diffusion can play a significant role [10]. Thus, for small Re, the above correlation breaks down such that $(H_s / d) \times \mathrm{Ri}^{1/2}$ increases excessively large with decreasing Re, since $\mathrm{Ri} \sim U_{F,o}^{-2}$. Note that the above correlation has the limiting behavior of $H_s \to 0$ as $U_{F,o} \to 0$.

In this regard, (H_s / d) is plotted in terms of Re in Fig. 11. The large Re correlation of Eq. (2) is also plotted and is

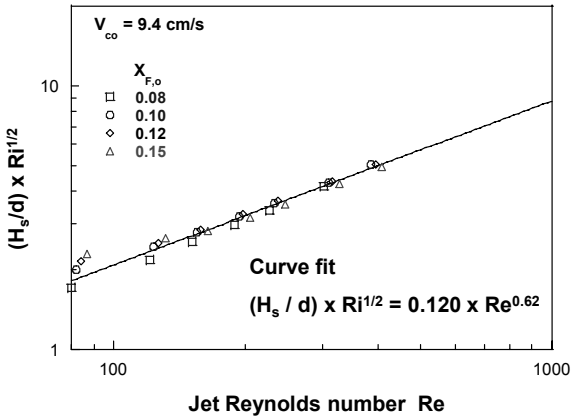

Fig. 10. Dimensionless stagnation height scaled with Richardson number in terms of jet Reynolds number for Re > 80.

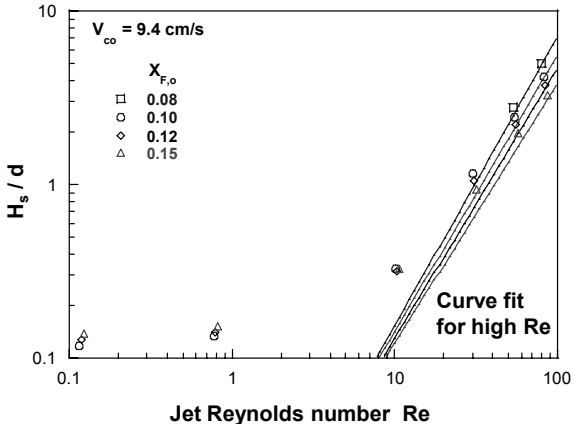

Fig. 11. Small Reynolds number behavior of stagnation height.

spreading out because of $\Delta\rho$ variation with $X_{F,o}$. The numerical results predict that the stagnation height approaches a non-zero constant as the Reynolds number approaches zero. The limiting constant values are near 0.12 d and are relatively insensitive to $X_{F,o}$. These characteristics can be attributed to the following. As $\mathrm{Re} \to 0$, the Peclet number defined in terms of the fuel diffusivity D, $\mathrm{Pe} = (U_{F,o} d) / D$, approaches zero, implying that the streamwise diffusion of fuel becomes important. Since, the buoyancy effect can be small since the volume to be influenced becomes small, the stagnation height will be influenced by the streamwise diffusion of fuel. The hydrodynamic behavior of coflow will be also important. In the limit of $U_{F,o} = 0$, a wake can be formed near the nozzle tip by the coflow. This behavior is demonstrated in Fig. 12, where the streamlines and velocity field (a) and fuel concentration field (b) are plotted. The streamlines clearly indicates the existence of the wake region near the nozzle exit, by having a recirculation zone. In the recirculation zone, the velocity is very small, thus the streamwise diffusion controls the stagnation height H_s for small Re, and thus H_s approaches a constant having non-zero value.

3.3 Coflow effect

The effect of coflow velocity on the stagnation height is investigated. Fig. 13 shows the stagnation height variation with coflow velocity at several fuel jet velocities. Here, the stagnation height is normalized with the height when $V_{co} = U_{F,o}$. The results demonstrate that the stagnation height is relatively insensitive to the variation of coflow velocity for a specified $U_{F,o}$. The stagnation height shows maximum when $V_{co} = U_{F,o}$, in such a way that H_s increases (decreases) with V_{co} for $V_{co} < U_{F,o}$ ($V_{co} > U_{F,o}$). In the present calculation, the stagnation region disappears when V_{co} is approximately over 20 cm/s by the strong coflow momentum.

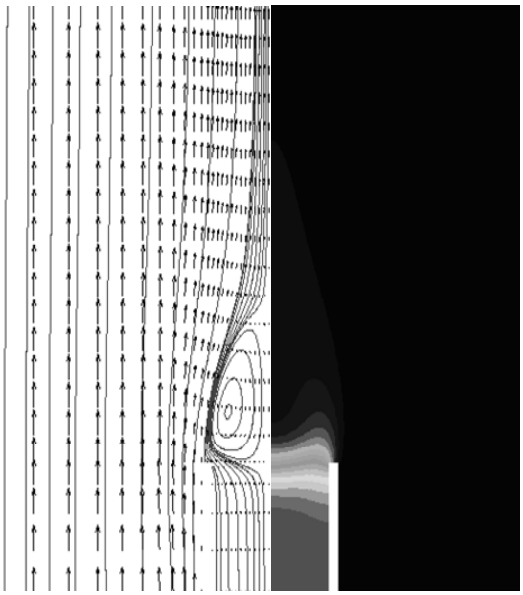

(a) (b)

Fig. 12. Profiles of concentration (a), streamline (b) and vorticity (c) ($X_{F,o}$ = 0.10, $U_{F,o}$ = 0.10 cm/s and V_{co} = 9.4 cm/s).

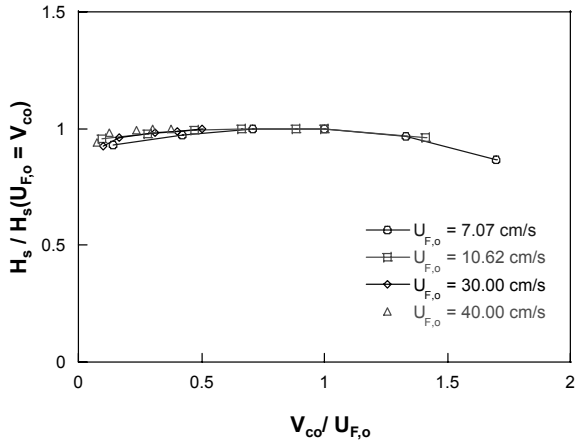

Fig. 13. Variation of stagnation height with coflow velocity at several fixed fuel velocities.

4. Concluding remarks

The characteristics of propane jets diluted with nitrogen have been investigated both numerically and experimentally. The Mie scattering and acetone PLIF techniques have been adopted to visualize the flow and concentration fields. The buoyancy effect significantly influences the velocity and concentration fields, when the molecular weight of fuel stream is heavier than that of air. By the gravitational deceleration, the mixture reaches a certain height and a stagnation region is formed. Then, the mixture was carried downstream by coflow air along the shear layer by having a cone shape. When the fuel jet velocity and/or the fuel mole fraction increase, the stagnation height oscillates and discrete vortices are observed due to the Kelvin-Helmholtz type instability in the shear layer region.

In the moderately large Reynolds number region of Re > 80, the stagnation height can be correlated as $(H_s/d)^2 \mathrm{Ri}^{1/2} \sim \mathrm{Re}^{0.62}$, which implies that the stagnation height is affected by the jet momentum and the buoyancy by the density difference between fuel and air. For small Reynolds numbers, the stagnation height is influenced by the streamwise diffusion of fuel near the lower stagnation region of the wake formed near the nozzle tip. Accordingly, stagnation height approaches non-zero constant values which were found to be relatively insensitive to fuel mole fraction. At a fixed fuel jet velocity, the stagnation height varies with coflow velocity, however, it is relatively insensitive to the variation of coflow velocity.

Acknowledgements

This work was supported by the Combustion Engineering Research Center. KWC, JK, and SHW were partially supported by the BK- 21 Program.

References

[1] T. Plessing, T. Terhoevven, N. Peters and M. S. Mansour, An experimental and numerical study of a liminar triple flame, *Combustion and Flame*, 115 (1998) 335-353.

[2] S. H. Won, S. H. Chung, M. S. Cha and B. J. Lee, Lifted flame stabilization in developing and developed regions of coflow jets for highly diluted propane, *Proc. Combust. Inst.*, 28 (2000) 2093-2099.

[3] J. Y. Hwang, W. Lee, G. G. Kang and S. H. Chung, Synergistic effect of ethylene-propane mixture on soot formation in laminar diffusion flames, *Combustion and Flame*, 114 (1998) 370-380.

[4] J. Kim, S. H. Won, M. K. Shin and S. H. Chung, Numerical simulation of oscillating lifted flames in coflow jets with highly diluted propane, *Proc. Combust. Inst.*, 29 (2002) 1589-1595.

[5] J. Kim, K. N. Kim, O. Fujita, J. Takahashi and S. H. Chung, Numerical simulation and parabolic flight test on oscillating lifted flames in coflow jets with gravity level variation, *Combustion and Flame*, 145 (2006) 181-193.

[6] S. Mahalingam, B. J. Cantwell and J. H. Ferziger, Nonpremixed combustion : full numerical simulation of a coflowing axisymmetric jet, inviscid and viscous stability analysis, Report TF-43, Thermosciences Division, Stanford University, Stanford, CA., (1989).

[7] H. N. Najm, P. S. Wyckoff and O. M. Knio, A semi-implicit numerical scheme for reacting flow (I. Stiff Chemistry), *J. Comput. Phy.*, 143 (1998) 381-402.

[8] R. J. Kee, F. M. Rupley and J. A. Miller, CHEMKIN-II : A fortran chemical kinetics package for the analysis of gas-phase chemical kinetics, Sandia National Laboratories Report, SAND89-8009, (1989).

[9] R. J. Kee, J. Warnatz and J. A. Miller, A fortran computer code package for the evaluation of gas-phase viscosities, conductivities, and diffusion coefficients, Sandia National Laboratories Report, SAND 83-8209, (1983).

[10] S. H. Chung and C. K. Law, Burke-Schumann flame with streamwise and preferential diffusion, *Combust. Sci. Technol.*, 37 (1984) 21-46.

Suk Ho Chung received his B. S. degree in Mechanical Engineering in 1976 from Seoul National University, and his M.S. and Ph. D. degree in Mechanical Engineering in 1980 and 1983, respectively from Northwestern University. He is a professor since 1984 in the school of Mechanical Aerospace Engineering, Seoul National University. His research interests cover combustion fundamentals, pollution formation, and lase diagnostics.